BIOCHEMISTRY
including biophysical chemistry & molecular biology

Article

pubs.acs.org/biochemistry

Aggregation of Alzheimer's Amyloid β-Peptide in Biological Membranes: A Molecular Dynamics Study†

Justin A. Lemkul* and David R. Bevan

Department of Biochemistry, Virginia Polytechnic Institute and State University, Blacksburg, Virginia 24061, United States

Supporting Information

ABSTRACT: Numerous studies have concluded that the interaction of the amyloid β-peptide (Aβ) and cellular membranes contributes to the toxicity and cell death observed in the progression of Alzheimer's disease. Aggregated Aβ species disrupt membranes, leading to physical instability and ion leakage. Further, the presence of Aβ on the membrane surface increases the aggregation rate of the peptide, as diffusion occurs in two dimensions, increasing the probability of interpeptide interactions. Molecular dynamics (MD) simulations have been used to investigate Aβ in a number of environments, including aqueous solution and membranes. We previously showed that monomeric $A\beta_{40}$ remains embedded in membranes composed of the most common lipids found in the cell membrane, but that the presence of ganglioside GM1 promotes release of the peptide into the extracellular medium. Here, we explore the interactions of two $A\beta_{40}$ peptides in model membranes to understand whether aggregation can occur prior to the release of the peptide into the aqueous environment. We found that aggregation occurred, to different extents, in each of the model membranes and that the aggregates, once formed, did not exit the membrane environment. This information may have important implications for understanding the affinity of Aβ for membranes and the mechanism of Aβ toxicity in Alzheimer's disease.

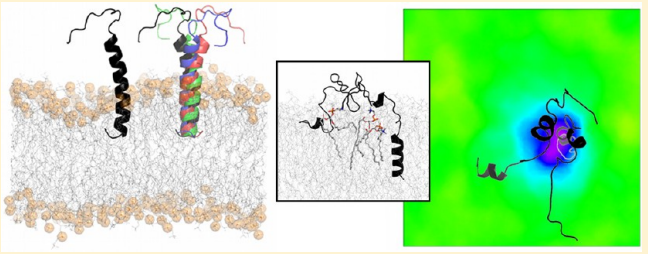

Alzheimer's disease is a progressive neurodegenerative disorder that affects over 5 million individuals in the United States and over 25 million worldwide[1] and is the leading cause of senile dementia. The principal histological lesions for this disease are extracellular plaques of the amyloid β-peptide (Aβ) and intracellular neurofibrillary tangles of the microtubule-associated protein tau. The discovery of Aβ as the principal component of the extracellular plaques led to the formation of the "amyloid hypothesis",[2] which states that Aβ is the primary toxic entity in Alzheimer's disease, especially through its associations with cellular membranes.[3,4]

Aβ is produced from the amyloid precursor protein (APP) by sequential proteolysis steps carried out by β-secretase in the endosomal pathway and γ-secretase in the plasma membrane.[5,6] The resulting Aβ peptides contain between 39 and 43 residues, with the 40- and 42-residue variants ($A\beta_{40}$ and $A\beta_{42}$, respectively) being the most common. The final proteolysis step (carried out by γ-secretase) occurs in lipid raft microdomains of the plasma membrane.[7] Thus, upon production, Aβ is exposed to a lipid matrix containing primarily glycolipids, cholesterol, and saturated lipids. In our previous work,[8−10] we concluded that monomeric $A\beta_{40}$ remained stably inserted in membranes composed of dipalmitoylphosphatidylcholine (DPPC), palmitoyloleoylphosphatidylcholine (POPC), palmitoyloleoylphosphatidylserine (POPS), an equimolar mixture of POPC and palmitoyloleoylethanolamine (POPE), and lipid rafts composed of a 1:1:1 molar ratio of POPC/palmitoylsphingomyelin (PSM)/cholesterol but exited raft membranes containing ganglioside GM1. Our results identified ganglioside GM1 as an important contributor to the early stages of the Aβ aggregation cascade.

Since the principal toxic species in Alzheimer's disease is believed to be soluble, oligomeric Aβ,[3,4,11,12] it is important to understand the early events in the aggregation cascade and the role that lipid membranes may play in the aggregation process. In solution, Aβ aggregation occurs through diffusion in three spatial dimensions. When associated with membranes, the diffusion is limited to two dimensions, in the plane of the membrane, thus enhancing the rate at which Aβ will aggregate.[13,14] Though aggregation in membranes has been demonstrated *in vitro* using a variety of model lipid bilayers,[13,15−18] it is unknown if Aβ can aggregate in membranes *in vivo* prior to its release into the extracellular medium and destabilize the plasma membrane in the process. Here, we apply molecular dynamics (MD) simulations in an effort to provide new insight into this process.

Recent MD simulations by Zhao et al.[19] showed that $A\beta_{42}$ can aggregate in a model DPPC/cholesterol membrane and that the aggregated peptides remain embedded in the membrane; that is, they do not exit the lipid bilayer and enter the aqueous phase. Zhang et al. recently studied the interactions of Aβ with Langmuir films and liposomes to demonstrate that Aβ aggregation in water and in membranes

Received: May 2, 2013
Revised: June 25, 2013
Published: July 2, 2013

   dx.doi.org/10.1021/bi400562x | *Biochemistry* 2013, 52, 4971−4980

are competing processes that are fundamentally different.[16] That is, monomeric Aβ prefers to partition into membranes where aggregation then occurs. Conversely, preformed aggregates of Aβ do not effectively enter into membranes. Thus, toxic aggregates can be formed within the membrane and lead to damage and ultimately cell death. These studies provide the basis for our present work, as the exact mechanism of Aβ aggregation within membranes is still unknown and the dependence of this process on lipid properties remains to be explored.

In the present work, we sought to expand upon the current understanding of Aβ-membrane interactions in the context of peptide aggregation. We posed several questions. First, do Aβ_{40} monomers form aggregates within the membrane, and if so, is there any dependence on lipid composition in this process? Second, what is the nature of the interpeptide interactions, in terms of both residues involved in aggregation and any secondary structure changes? Finally, does Aβ_{40} aggregation adversely affect the structure of the lipid membrane? The application of atomistic MD simulations allows us to probe these events in great detail.

METHODS

The starting configuration for the Aβ_{40} peptide was taken from work by Coles et al.,[20] which we have used in our previous studies on Aβ-membrane interactions.[8−10] The coordinates and topologies for the membranes used in this work (POPC, POPS, POPC/POPE, and rafts) were taken from previous studies,[21−25] with coordinate files expanded as needed in the $x-y$ plane to produce membranes of suitable dimensions for the insertion of two peptides. Contents and dimensions of the simulation systems are given in Table 1. The force field applied to the Aβ_{40} peptide was GROMOS96 53A6.[26] These peptides were placed diagonally from one another in the $x-y$ plane of the membrane with a center-of-mass (COM) distance of 3.3 nm and a minimum distance between any pair of atoms of approximately 1.0 nm (Figure 1). This orientation produced what we called "Pose 1." Three additional poses were generated by successively rotating peptide 2 by 90° about the z-axis while keeping peptide 1 fixed (Figure 1B). The initial COM distances between the two peptides for Poses 2, 3, and 4 were 3.7, 4.2, and 3.9 nm, respectively. Minimum interpeptide distances between any atom pairs in Poses 2, 3, and 4 were 2.0, 2.2, and 2.4 nm, respectively. These proteins were then inserted into the membranes using the InflateGRO methodology.[27]

All further preparation steps and simulations were carried out using the GROMACS package,[28] version 4.0.7. Following insertion of the peptides into the lipid membrane, the unit cell was filled with SPC water[29] and ∼150 mM NaCl, including 4 or 6 Na^+ counterions to balance the net charge on each of the Aβ_{40} peptides, depending upon the protonation state (see below). Each system was energy-minimized using the steepest descent algorithm and was subsequently equilibrated in three phases. During all phases of equilibration, position restraints (using k_{pr} = 1000 kJ mol^{-1} nm^{-2}) were applied to all protein heavy atoms. For the first phase of equilibration, an NVT ensemble was applied, and the system equilibrated at 100 K. The Berendsen weak coupling algorithm[30] was used to control the temperature of the system. The peptides, lipids, and solvent (including ions) were coupled separately. NVT equilibration was carried out for 100 ps. Following NVT, each system was linearly heated from 100 to 310 K over 1 ns using an NPT ensemble at 1 bar of pressure. During this process, the Berendsen algorithm[30] was used to control both temperature and pressure. For the final phase of equilibration, an NPT ensemble was maintained at 310 K and 1 bar using the Nosé−Hoover thermostat[31,32] and Parrinello−Rahman barostat.[33,34]

Table 1. Contents of the Simulated Systems

membrane	lipid content	dimensions (nm)[a]
POPC	250 POPC	8.75 × 8.75 × 12
POPS	246 POPS	8.5 × 8.5 × 12
POPC/POPE	140 POPC, 140 POPE	9.94 × 9.94 × 12
Raft	127 POPC, 113 PSM, 121 cholesterol	8.73 × 8.73 × 12
GM1-Raft	125 POPC, 92 PSM, 119 cholesterol, 24 GM1	8.75 × 8.75 × 12

[a]Dimensions given ($x \times y \times z$) are those of the energy-minimized systems, i.e., prior to equilibration or further simulation.

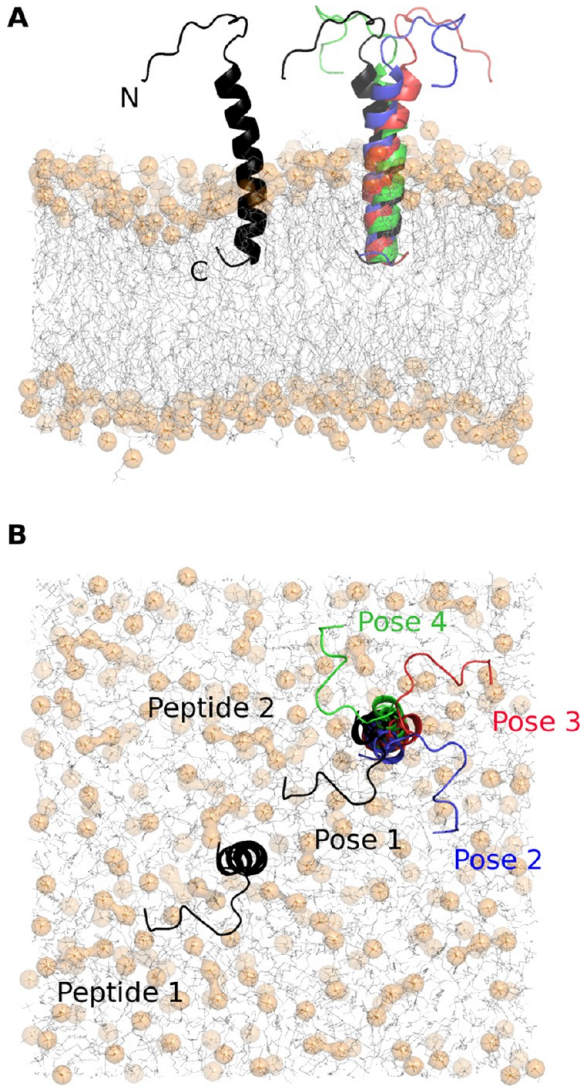

Figure 1. Starting configurations of the four poses (labeled numerically) of the Aβ_{40}-POPC system, as viewed (A) through the $x-y$ plane and (B) along the z-axis. The N- and C-termini of peptide 1 are indicated for perspective; peptide 2 has an analogous orientation. The different poses in panel B are labeled by color. The peptides are shown in cartoon representation. Lipids are shown as gray lines with phosphorus atoms indicated by translucent gold spheres.

Production MD simulations were carried out for 200 ns using this same ensemble, in the absence of any restraints. Three replicate simulations were conducted for each system, initiated using different random starting velocities at the outset of NVT equilibration. The approach of using four starting configurations with three replicates for each allowed us to obtain 2.4 μs of sampling in each simulation set.

Simulations were carried out with constraints on all bonds using the P-LINCS algorithm,[35] allowing an integration time step of 2 fs. Long-range electrostatic interactions were calculated using the smooth particle mesh Ewald (PME) method.[36,37] All short-range nonbonded interactions (including van der Waals terms and the real-space contribution to PME) were truncated at 1.2 nm. The neighbor list was updated every 5 simulation steps. Dispersion correction was applied to energy and pressure terms to account for finite truncation of van der Waals interactions. Analysis was conducted using programs within GROMACS or with our own software, GridMAT-MD.[38] Secondary structure was assigned using the DSSP algorithm.[39]

Throughout this paper, simulations are referred to by the lipid type (POPC, POPS, POPC/POPE, Raft, and GM1-Raft) and the C-terminal protonation state of the Aβ_{40} peptide. Thus, peptides with protonated C-termini are called "CH" (with a net charge of −2 on each peptide), and those with ionized C-termini are called "CI" (net charge of −3). Both protonation states were considered for reasons described previously.[8,10] The N-termini of all peptides were treated as positively charged. Individual simulations within a set are assigned a numeral. For instance, simulation POPC-CH-1.3 would indicate replicate 3 of Pose 1 within the set of simulations conducted in POPC with peptides containing protonated C-termini. Thus, in total, 120 simulations (12 each within 10 simulation sets) were carried out.

RESULTS AND DISCUSSION

Of interest in this work were several points related to both Aβ aggregation and the effects this process may have on the structure of the surrounding membrane and the dynamics of the peptides themselves. In this regard, we analyze (i) aggregate formation, (ii) position and orientation of Aβ_{40} within the membrane, (iii) secondary structure of Aβ_{40}, and (iv) membrane structure.

We begin the discussion of our findings with several important caveats. The starting structure for Aβ_{40} was determined in the presence of SDS micelles[20] and as such may not correspond directly to the structure of the peptide *in vivo*. We do believe, however, that this structure is a reasonable approximation of the structure of Aβ_{40} upon its release from the γ-secretase complex, as the domain of APP containing the Aβ sequence is a single-pass transmembrane helix, and it is likely that much of the Aβ_{40} structure is helical upon its generation. The initial placement of the two Aβ_{40} peptides in the systems constructed here is also arbitrary; an infinite set of configurations could be generated for the starting structure based on different rotational and translational transformations to the peptide structures. The starting configurations used here were simple constructs that enabled us to build systems of minimal size, to allow for longer simulations in a reasonable amount of time. It is important to state that the time frame explored in each of these simulations (200 ns) is short by physiological standards, but very long by computational metrics. Recent work by Zhao et al.[19] simulated an Aβ trimer for 1 μs, but they conducted only one simulation. Our approach of using multiple 200-ns simulations provides greater statistical confidence in the results we have obtained. The accumulated sampling time for each system is 2.4 μs and includes results from four different starting configurations.

As a final note, it is important to consider the effect that the chosen force field will have on the outcome of the study. Different molecular mechanics force fields have different underlying parametrization strategies and have been validated in different ways. Recent work has shown that many force fields overly bias helical structures,[40] while the GROMOS96 53A6 parameter set,[26] employed here, may overstabilize extended configurations and understabilize helices.[41] Very recently, Olubiyi and Strodel demonstrated that GROMOS96 53A6 reproduced calculated NMR shifts for Aβ,[42] indicating that the structures it produces are compatible with experimental observations. We elected to use GROMOS96 53A6 because it is the force field used in our previous work over the past several years,[8−10] is compatible with a popular united-atom lipid force field[21] that allows for faster calculations by reducing the degrees of freedom, and has recently been shown to be sufficiently accurate for studies of Aβ.[42]

Aggregation of Aβ_{40} Peptides. We defined a peptide aggregate as occurring when a minimum of 100 interpeptide heavy atom contacts persisted over the final 100 ns of each simulation, and the $x-y$ COM distance between the peptides was within 2.75 nm. This distance was determined on the basis of a qualitative assessment of the interactions established during the simulations and further justified on the basis of the rate of diffusion necessary to produce such a distance. The total displacement from the initial configurations that would be needed to achieve this final COM separation would suggest lateral diffusion on the order of 1−6 cm^2 s^{-1}, which is in the range of normal lipid diffusion.

Simulations in which the Aβ_{40} peptides satisfied the distance and contact criteria were called "strong" aggregates (Figure 2A); in cases in which the contact criterion was met but the COM distance criterion was not or wherein the COM distance criterion was met and a non-zero number of contacts (but fewer than 100) formed, the resulting aggregates were called "weak" (Figure 2B). Weak aggregates generally represent situations in which the Aβ_{40} peptides adopted elongated structures that formed interactions without large changes in COM distance. Strong aggregates formed at close distance and established a greater number of contacts. We note that most aggregates that formed produced peptides with a COM distance well below the 2.75-nm cutoff, indicating that they diffused more quickly than the surrounding lipids and thus the interactions enhanced the attraction between the peptides.

Dimers formed in all of the membrane systems explored here, to different extents depending upon lipid type (Table 2). The simulations of Aβ_{40} in POPC produced aggregates in 50% of the simulations, eight strong (four each in the POPC-CH and POPC-CI sets) and four weak aggregates (three in the POPC-CH set and one in the POPC-CI set). Simulations of Aβ_{40} in POPS produced aggregates in only 25% of the simulations, three strong (one in the POPS-CH set and two in the POPC-CI set) and three weak (in POPS-CH). In the POPC/POPE-CI set, aggregates formed in 29.2% of the simulations, including six strong aggregates (four in POPC/POPE-CH and two in POPC/POPE-CI) and only one weak aggregate (in the POPC/POPE-CI set). Thus, for these three simple model membranes, it appears that the ability of Aβ_{40} to aggregate can be expressed as a function of hydrogen bonding

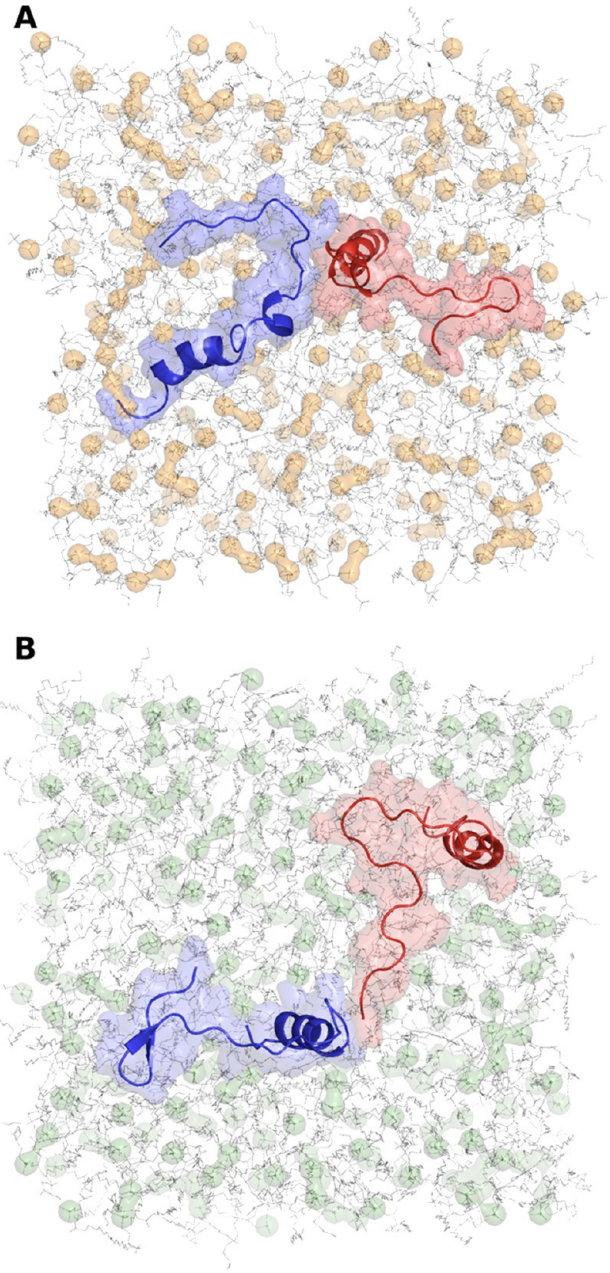

Figure 2. Examples of (A) a "strong" aggregate, from the POPC-CH-3.3 trajectory and (B) a "weak" aggregate, from the POPS-CH-1.1 trajectory. Each peptide is shown with an overlaid translucent surface to give an impression of the overall shape of the molecules. Lipids are shown as gray lines, with phosphorus atoms indicated by translucent gold (POPC) or green (POPS) spheres.

potential between the peptides and the surrounding lipids. Lipids with greater numbers of hydrogen bonding groups such as POPS impeded Aβ_{40} aggregation to the greatest extent. The presence of POPE in the POPC/POPE membrane also impeded aggregation, but not as strongly as in the case of POPS. The time taken to form aggregates is shown in Table 2, and Aβ-lipid hydrogen bonds for the different systems simulated here are summarized in Table 3. The membrane that caused Aβ_{40} aggregates to form the slowest was POPS. POPC and POPC/POPE were nearly equivalent, but the greater number of aggregates observed in POPC reinforces the conclusion that hydrogen bonding impedes aggregate formation. The aggregates that formed in POPC/POPE did so as quickly as the aggregates formed in POPC, but there were far fewer aggregates overall in POPC/POPE.

Table 2. Quantification of Aggregates Formed; Twelve Simulations Were Performed in Each Set

	dimers formed				
system	strong	weak	total	av COM distance (nm)[a]	av formation time (ns)[b]
POPC-CH	4	3	7	2.4 ± 0.5	17 ± 21
POPC-CI	4	1	5	2.2 ± 0.6	9 ± 9
POPS-CH	1	3	4	3.2 ± 0.8	26 ± 35
POPS-CI	2	0	2	2.4 ± 0.4	22 ± 4
POPC/POPE-CH	2	0	2	2.5 ± 0.3	8 ± 6
POPC/POPE-CI	4	1	5	2.3 ± 0.2	13 ± 23
Raft-CH	4	0	4	1.9 ± 0.9	15 ± 21
Raft-CI	4	2	6	2.5 ± 0.7	3 ± 3
GM1-Raft-CH	3	0	3	1.9 ± 0.4	4 ± 2
GM1-Raft-CI	2	1	3	2.2 ± 0.8	4 ± 3

[a]Average interpeptide COM distance in all systems in which aggregates formed (both strong and weak) over the last 100 ns of simulation time. [b]Time at which the minimum threshold for contacts formed was reached, considering all systems in which aggregates formed.

The Aβ_{40} peptides formed aggregates in the raft environment without GM1 in 41.7% of the simulations. In the 12 Raft-CH simulations, four strong aggregates formed. In the Raft-CI set, four simulations produced strong aggregates and two produced weak aggregates. In the GM1-Raft systems, in which aggregates formed in 25% of the simulations overall, the GM1-Raft-CH set produced three strong aggregates, and the GM1-Raft-CI set produced two strong aggregates and one weak aggregate. These results are not unexpected, given the fact that most of the lipids in the raft (both POPC and PSM) contained PC headgroups. The Aβ_{40} peptides formed comparable numbers of hydrogen bonds with PC-containing phospholipids in the POPC and Raft simulations. Thus, the mobility of these peptides and their potential for interaction was comparable in these environments (also indicated by the similarity between aggregate formation time shown in Table 2), allowing aggregates to form with a greater frequency and strength than in the POPS and POPC/POPE systems. Fewer aggregates were observed in the GM1-Raft systems relative to the Raft systems, likely due to the extensive hydrogen bonding interactions that emerged between Aβ_{40} and GM1 (Table 3). The aggregates that arose in GM1-Raft simulations formed the fastest of all the membrane environments (Table 2), however, indicating that perhaps even more sampling and starting configurations may be necessary to determine the effect of the initial placement of GM1 molecules relative to the Aβ_{40} peptides. Aggregates that formed did so very rapidly (within approximately 4 ns for both GM1-Raft-CH and GM1-Raft-CI systems), while peptides in other replicates never formed any contacts and/or did not diffuse very far from their initial positions.

The interactions formed between Aβ_{40} peptides upon aggregation were principally between residues in the N-terminal regions of the peptide. The C-terminal hydrophobic residues generally remained far apart, forming few, if any, direct contacts within the membrane core. To quantify these interactions, an average distance matrix was constructed from the final snapshot of each simulation in which an aggregate (strong or weak) formed (Figure 3). It can be seen that no interactions formed

dx.doi.org/10.1021/bi400562x | *Biochemistry* 2013, 52, 4971−4980

Table 3. $A\beta_{40}$–Lipid Hydrogen Bonds[a]

system	POPC	POPS	POPE	PSM	Chol	GM1
POPC-CH	26 ± 5					
POPC-CI	24 ± 5					
POPS-CH		44 ± 6				
POPS-CI		45 ± 8				
POPC/POPE-CH	18 ± 4		26 ± 4			
POPC/POPE-CI	16 ± 1		28 ± 5			
Raft-CH	15 ± 4			11 ± 2	2 ± 2	
Raft-CI	15 ± 5			11 ± 3	3 ± 2	
GM1-Raft-CH	12 ± 4			4 ± 2	0.8 ± 0.5	14 ± 4
GM1-Raft-CI	13 ± 4			4 ± 3	1 ± 1	14 ± 5

[a]Data are averaged over the final 100 ns of each trajectory, considering both peptides in all simulation sets. Shown are the resulting averages with standard deviations.

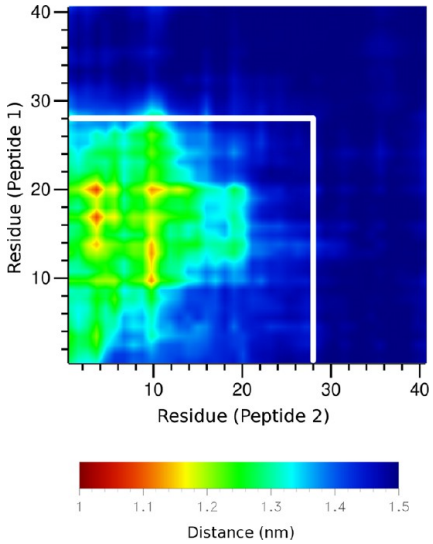

Figure 3. Average distance matrix for all trajectories in which aggregates formed. The distance matrix represents the mean smallest distance between all residue pairs and was constructed from the final configuration of each trajectory as representative of each simulation. Residues enclosed in the white box indicate the N-terminal polar region that is initially exposed to the aqueous solvent in each simulation.

outside of the polar N-terminal residues (contained within the white outline in Figure 3). These findings are in good agreement with recent experiments conducted by Zhang et al.,[16] who found that Aβ aggregation in membranes was driven principally by residues 11–16 of the Aβ sequence. Contacts involving these residues were frequent in our simulations (Figure 3). They further determined that the hydrophobic C-terminal residues, while important for aggregation of Aβ in the extracellular medium, were not involved in aggregation within the membrane; rather, these residues served to anchor the peptide in the membrane. Our results agree with these observations, since few, if any, contacts emerged involving these residues (Figure 3). We can conclude from our results that the protonation state of the $A\beta_{40}$ peptides (CH or CI) has little to no impact on the ability of the peptides to form aggregates, further emphasizing the role of N-terminal residues, not C-terminal residues, in aggregation within the membrane. C-terminal protonation state does play an important role in the position and orientation of the peptides within the membrane and will be discussed in detail in the next section.

We conclude this section by noting that the ability of $A\beta_{40}$ to form aggregates within the membrane was not biased due to the starting configurations. Though many orientations exist as possible starting configurations for these systems, we have attempted to eliminate bias toward certain interactions by producing four orientations that begin with the peptides rotated with respect to one another. The fact that aggregates can arise from any of these initial configurations gives confidence in the results presented here.

Position and Orientation of $A\beta_{40}$ in Membranes. In our previous work,[10] we found that monomeric $A\beta_{40}$ interacted with GM1 in a manner that promoted the exit of the peptide from the membrane, a behavior that was not observed in the simulations of $A\beta_{40}$ in the other model membranes. Thus, it was of interest in the present work to determine if the ability of $A\beta_{40}$ to aggregate affected its exit from the membrane. We previously defined an "exit" from the membrane as occurring when the COM of residues 29–40 of $A\beta_{40}$ (initially embedded in the membrane) crossed above the average phosphate plane of the extracellular leaflet of the membrane. We utilize that same definition here. We have quantified the position and orientation of the $A\beta_{40}$ peptide within each model membrane using two criteria: (i) the tilt angle of the principal axis through residues 29–40 and the z-axis and (ii) the distance between the COM of residues 29–40 and the average phosphate plane. Results of these calculations are summarized in Table 4, and images of the positions of $A\beta_{40}$ within all membrane systems are presented in Supporting Figures S1–S10. Histograms that

Table 4. Tilt Angle and z-Axis Position of $A\beta_{40}$ Peptides in Model Membranes[a]

system	tilt angle (deg)	relative position (nm)
POPC-CH	47 ± 28	−1.5 ± 0.6
POPC-CI	85 ± 30	−1.1 ± 0.5
POPS-CH	29 ± 18	−1.4 ± 0.3
POPS-CI	96 ± 20	−1.0 ± 0.2
POPC/POPE-CH	63 ± 21	−0.9 ± 0.2
POPC/POPE-CI	77 ± 18	−0.6 ± 0.3
Raft-CH	56 ± 25	−1.0 ± 0.3
Raft-CI	77 ± 21	−0.5 ± 0.2
GM1-Raft-CH	61 ± 21	−0.8 ± 0.3
GM1-Raft-CI	85 ± 24	−0.5 ± 0.2

[a]Averages (with standard deviations) were calculated for both peptides in each system, averaged over the final 100 ns of each trajectory.

dx.doi.org/10.1021/bi400562x | Biochemistry 2013, 52, 4971–4980

Table 5. Secondary Structure Content of $A\beta_{40}$ Peptides, Averaged over the Last 100 ns of Simulation Time[a]

system	coil	β-strand[b]	bend	turn	total helix[c]
POPC-CH	36 ± 4	3 ± 3	17 ± 3	10 ± 5	34 ± 6
POPC-CI	38 ± 6	4 ± 3	17 ± 4	13 ± 4	28 ± 8
POPS-CH	34 ± 5	5 ± 4	18 ± 4	15 ± 4	29 ± 7
POPS-CI	40 ± 7	6 ± 4	19 ± 5	12 ± 5	23 ± 10
POPC/POPE-CH	39 ± 6	4 ± 3	20 ± 4	14 ± 5	23 ± 10
POPC/POPE-CI	41 ± 7	4 ± 5	19 ± 5	12 ± 4	23 ± 10
Raft-CH	36 ± 5	6 ± 4	20 ± 3	13 ± 5	25 ± 7
Raft-CI	44 ± 8	6 ± 5	23 ± 5	13 ± 4	14 ± 9
GM1-Raft-CH	43 ± 6	6 ± 4	21 ± 5	13 ± 4	16 ± 6
GM1-Raft-CI	45 ± 5	7 ± 5	26 ± 5	13 ± 5	9 ± 6

[a]Percentages are shown with standard deviations. [b]β-strand content includes both extended β-sheet and isolated β-bridge conformations. [c]Total helix is the sum of α-, π-, and 3_{10}-helix content.

illustrate the distributions of relative COM distances are shown in Figures S11–S15.

The values observed for tilt angle and relative position are very similar to our previous results for monomeric $A\beta_{40}$ in these same membranes.[10] These results indicate that the presence of multiple peptides, aggregated or not, does not affect the intrinsic ability of $A\beta_{40}$ to tilt and rise toward the membrane–water interface. Peptides with deprotonated C-termini (model CI) are more proximal to the membrane–water interface in all membranes, with the protonated C-terminal peptides remaining 0.3–0.5 nm further into the hydrophobic membrane core (Table 4). The CI peptides tilted more extensively than the CH peptides, a result of their ionized termini being attracted more strongly to the polar membrane–water interface.

In the simulations of $A\beta_{40}$ in POPC, POPS, POPC/POPE, and Raft environments, none of the peptides ever exited the membrane, either in monomeric or aggregated form. Our previous work[8,10] suggested that $A\beta_{40}$ should remain embedded in a variety of membranes but that the presence of GM1 enhances the ability of $A\beta_{40}$ to exit from raft membranes. We do not observe such behavior here in the context of the GM1-Raft simulations to the same extent as in our previous work. In one simulation (GM1-CI-2.2), the C-terminal residues 29–40 of a single peptide remained coincident with the membrane–water interface over the final 100 ns, sampling configurations as far as 0.67 nm away from the membrane. Numerous other simulations produced peptides that transiently sampled configurations outside of the membrane (four in the GM1-Raft-CH set and nine in the GM1-Raft-CI set). Nearly all of these events occurred when the peptides were in monomeric form, indicating that the formation of aggregates within the membrane disfavors release of the peptides into the extracellular space, in agreement with the findings of Zhang et al.[16] We attribute the findings of the present work to the fact that there is only a small probability that complete exit will occur (30% in our previous work) and that aggregation should impede the ability of Aβ to exit the membrane, as Aβ monomers preferentially aggregate in the membrane rather than exit into the extracellular space.[16] We observed aggregation in 6 of the 24 simulations conducted here that included GM1 (Table 2). Whereas monomeric $A\beta_{40}$ may leave the membrane via interactions with GM1 and can lead to extracellular aggregation, the presence of multiple $A\beta_{40}$ peptides disfavors membrane release and instead leads to aggregation within the membrane. The effects of soluble Aβ binding to GM1 from the aqueous environment outside the cell remains a topic to be explored further in the future.

Secondary Structure of $A\beta_{40}$ Peptides. Previous structural and simulation studies of Aβ in membranes and membrane-mimicking environments have concluded that the peptide is principally helical, though some regions are disordered.[20,43,44] Our own results of monomeric $A\beta_{40}$ have shown that transient β-strand formation is observed in all membrane environments, but β-strand content is enhanced by the presence of GM1 clusters.[10] These GM1 clusters provide a polar, dehydrated environment that facilitates the formation of β-hairpin structures, principally within the N-terminal region of the peptide. Secondary structure content for the $A\beta_{40}$ peptides in the simulations conducted here is summarized in Table 5. Per-residue helical and strand probabilities are shown in Supporting Figures S16–S20. We focused our analysis on the final 100 ns of each trajectory, as $A\beta_{40}$ underwent some secondary structure changes over the first half of the trajectory.

In agreement with previous experimental and simulation data,[10,20,43−45] the principal secondary structure features of the $A\beta_{40}$ peptides were random coil and helix. We consider total helical content here, as in our previous work,[10] rather than individual α-helix, π-helix, and 3_{10}-helix elements, as the definition and balance of these structures is not well-defined for most force fields.[40,41,46] Helical structures were sampled between residues 15–23 and 28–38 (Supporting Figures S16–S20), in agreement with structural studies that have examined $A\beta_{40}$ in membrane-mimicking environments.[20] In general, we note that model CI peptides had lower helical content toward the C-terminus, likely due to helical instability that arises due to the ionized terminus. As summarized above, model CI peptides were generally closer to the membrane–water interface and thus underwent additional structural rearrangement. β-Strand content was highest for the simulations of $A\beta_{40}$ in Raft and GM1-Raft systems (Table 5), in agreement with our previous results.[10] The GM1-Raft systems produced the lowest total helical content, indicating that these peptides were the most disordered in these membrane systems, an attribute that may enhance aggregation. We note that helical content was reduced in the membrane-embedded C-terminal region in GM1-Raft systems (Supporting Figure S20) relative to the other membranes studied here. β-Strand occurrence was most frequent in the GM1-Raft systems, with short β-hairpins emerging at various locations within the $A\beta_{40}$ structures in 9 of 12 simulations in the GM1-Raft-CH set and 10 of 12 simulations in the GM1-Raft-CI set. Hairpins were most frequent within N-terminal residues 1–15 in all systems (Supporting Figures S16–S20). In GM1-Raft systems, the same β-hairpins formed with greater frequency, and additional

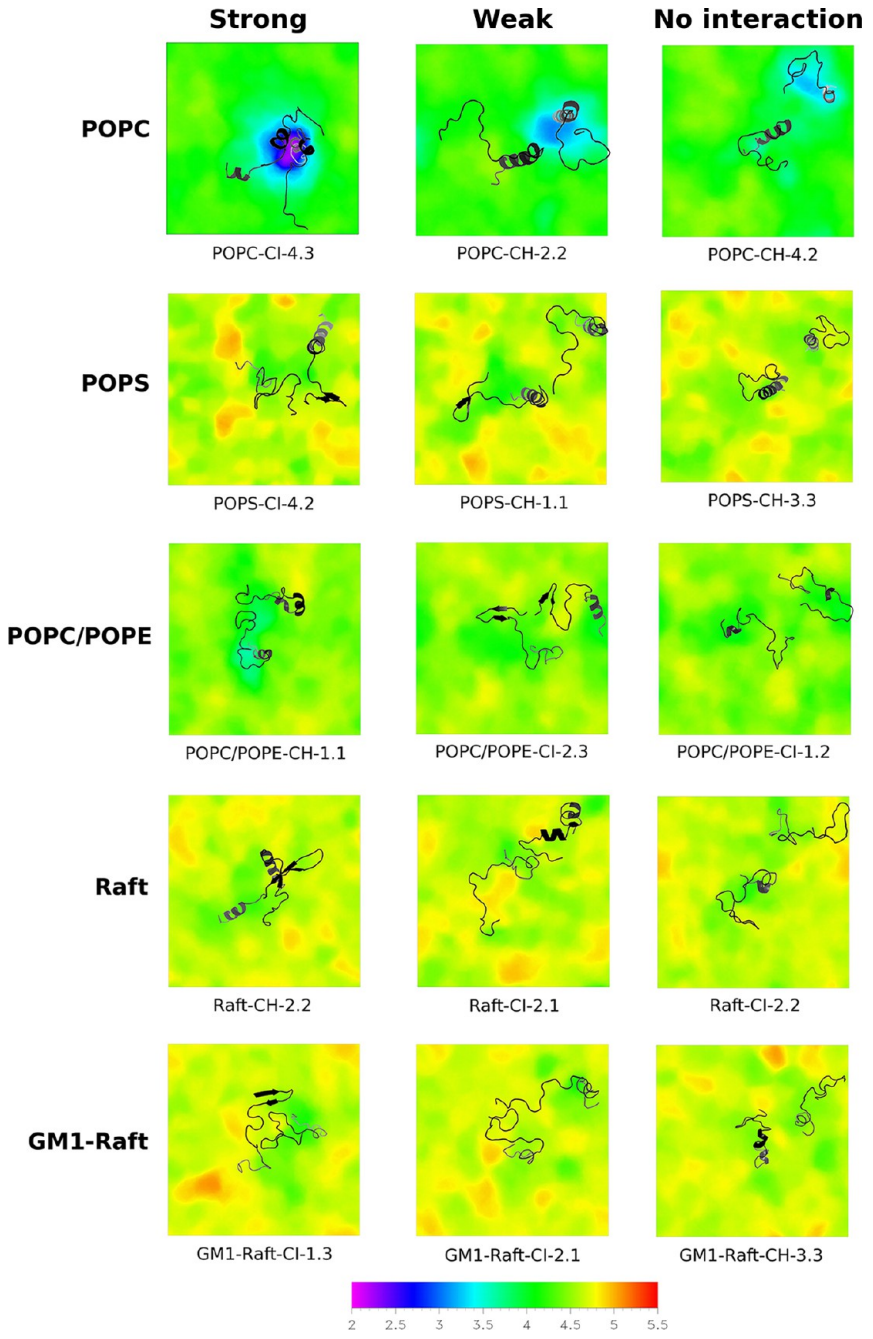

Figure 4. Membrane thickness projections in the $x-y$ plane, showing examples of strong and weak aggregates, as well as systems in which no interaction occurred. Thicknesses were calculated as the average over the last 50 ns of each trajectory, using snapshots every 1 ns. To define the membrane boundaries, phosphorus atoms were used as reference atoms for the GridMAT-MD calculations. Aβ_{40} structures are taken from the final configuration of each trajectory indicated and are colored as a black to gray gradient to imply depth within the membrane. Black regions indicate regions of the peptide near the membrane−water interface, while gray residues are within the bilayer interior. The legend represents thickness in nm.

β-hairpins formed in residues toward the middle of the Aβ_{40} sequence (residues 23−30) and toward the C-terminus (residues 30−40), as shown in Supporting Figure S20.

The fact that the secondary structure content of multiple Aβ_{40} peptides, including those that have aggregated, is similar to those in the monomeric state explored in our previous work suggests that Aβ_{40} aggregates do not form extensive β-strand structures and remain principally disordered at this stage in the aggregation cascade. Helical structures account for the next most prevalent secondary structural elements (Table 5). Structural studies have concluded that low-molecular weight Aβ aggregates are largely unstructured in solution, while only higher-order species form extensive β-strand structures.[47] Our results indicate that the same holds true for aggregates of Aβ_{40} formed within the membrane. Emergence of more elongated β-strands and intermolecular β-sheets may require the presence of a larger number of Aβ peptides, a topic that bears further examination in the future. Greater structural changes may also require complete exit of Aβ from the membrane into an aqueous environment, a process that may occur over longer time periods.

dx.doi.org/10.1021/bi400562x | *Biochemistry* 2013, 52, 4971−4980

Effect of Aβ_{40} Peptides on Membrane Structure. A central tenet of the "amyloid hypothesis" of Alzheimer's disease is the ability of Aβ to cause structural destabilization of cell membranes that ultimately leads to cell death. We sought to determine if the presence of multiple Aβ_{40} peptides, aggregated or not, could impart structural changes on the model membranes considered here. We quantified the membrane thickness along the *z*-axis for each system using GridMAT-MD.[38] Results are shown in Figure 4.

The most notable deformations occurred in the case of the POPC membranes. In the vicinity of the Aβ_{40} peptides, the membrane thickness was reduced in excess of 1.0 nm in many cases (Figure 4 and Supporting Figures S21 and S22) and up to 2.0 nm in the case of strong aggregate formation (Figure 5)

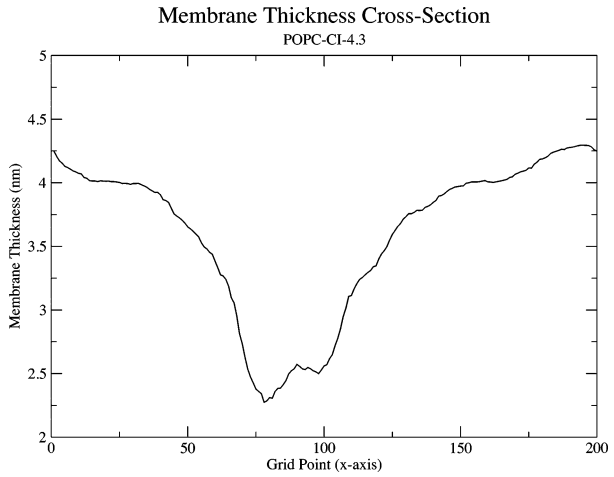

Figure 5. Cross-section of membrane thickness along the *x*-axis through the deepest invagination in the membrane in the POPC-CI-4.3 simulation.

relative to lipids found at the periphery of the unit cell. Such behavior is similar to our observations in the case of Aβ_{40} in DPPC.[9] Several of the simulations in the POPC/POPE-CH and POPC/POPE-CI systems produced similar results (Supporting Figures S21 and S22). It is apparent from our results that Aβ_{40}, even in its monomeric state, has an intrinsic ability to cause localized thinning of the membrane on the order of 0.5 nm or more. That is, small regions of thinning were observed even in the absence of aggregation. When aggregation occurred, the perturbed regions were much larger in terms of the lateral area of the membrane that was affected. The invaginations were deeper (1.0−2.0 nm) when aggregation occurred, and thus an additive effect of Aβ_{40} peptides on the membrane is proposed. While one Aβ_{40} peptide may cause localized thinning, aggregated peptides cause even more pronounced thinning.

Unlike POPC, the other membranes examined here were less susceptible to perturbation induced by Aβ_{40}. We attribute these findings to two factors: (i) the differing ability of lipid headgroups to form hydrogen bonds and (ii) the presence of cholesterol in the Raft and GM1-Raft simulation sets. Interactions between adjacent lipids, such as hydrogen bonding and hydrophobic packing of acyl chains, give rise to membrane structure and stability, and thus membranes that differ in these properties likely also differ in their response to Aβ_{40}.

Relative to the simulations of Aβ_{40} in POPC, the simulations of Aβ_{40} in POPC/POPE and POPS produced less pronounced thinning (0.5−0.7 nm, Figure 4 and Supporting Figures S23−S26). The phosphatidylethanolamine headgroup of the POPE lipids is characterized by a primary amine capable of hydrogen bonding to Aβ_{40} (Table 3), POPC, or other POPE lipids. Whereas Aβ_{40} tilted and caused POPC lipids to disorder, leading to bilayer thinning, the intermolecular interactions between POPC and POPE lipids made this membrane less susceptible to such structural change, as was also the case for the POPS membrane. The phosphatidylserine headgroup contains two hydrogen bond acceptors (phosphate and carboxylate) and a donor (primary amine), thus giving it the greatest per-lipid hydrogen bonding capacity of any of the lipids examined here. The structure of the POPS membranes remained very stable over the course of the simulations carried out here, indicating that greater hydrogen bonding capacity within the lipid headgroups can reduce the structural destabilization imparted by Aβ_{40}.

Previous work by Qiu et al. has suggested that the presence of cholesterol in the membrane acts to protect the bilayer from Aβ toxicity.[48] In our simulations in the Raft and GM1-Raft simulation sets, cholesterol was present in a nearly equimolar ratio with the phospholipids. In cell membranes, raft domains are more rigid and tightly packed than other regions and thus may be less susceptible to structural changes induced by the presence of Aβ. We observe this effect in our simulations with respect to deformations in the membrane. As was the case in POPC/POPE and POPS membranes, the Aβ_{40}-induced structural perturbations in Raft and GM1-Raft systems were minimal (Figure 4 and Supporting Figures S27−S30). Thus, it appears that raft domains serve dual functions in the context of Aβ. The first was proposed in our earlier work,[10] in which we found that monomeric Aβ_{40} could exit GM1-containing rafts. The second function, illustrated here, may be to concentrate Aβ, as we observed extensive formation of numerous aggregates in our simulations in both Raft and GM1-Raft simulation sets. These aggregates may then diffuse to other regions of the cell membrane rich in phosphatidylcholine-containing lipids and lacking cholesterol in order to destabilize the cell membrane, as has been proposed previously.[49]

Recent work by Poojari et al. has found that Aβ_{42} monomers and tetramers permit the leakage of water molecules across the membrane,[50] though the amount of water that crossed the membrane when Aβ_{42} was present was not increased relative to control membranes. In contrast, we do not observe this behavior in any of our simulations. Given that Poojari et al. report that water translocation was relatively fast (approximately 12 ns or less), we believe that we achieved adequate total sampling to observe this phenomenon if it had occurred. In fact, we report more total sampling in each simulation set than in the work of Poojari et al., who accumulated 500 ns of sampling time in their simulations. Thus, the only explanation for the absence of water permeation is conformational dependence. Poojari et al. reported water translocation in the case where Aβ was modeled as an elongated β-hairpin, but we observe no such structure or orientation in any of our simulations, though it is possible that Aβ_{42} could behave differently than Aβ_{40}, which we have used in our work. Further, the initial orientation for the helical model of Aβ in that study placed Lys16 at the membrane−water interface, whereas our initial position located Lys28 at the interface, such that all charged residues were exposed to water instead of the hydrophobic membrane interior. Although our early work suggested that Aβ_{40} might reorient itself such that Lys16 was

coincident with the membrane−water interface, this behavior only emerged when all titratable residues were protonated, thus emulating low pH. At physiological pH, we have not observed reorientation of $A\beta_{40}$, and no residue beyond Val24 has embedded in the membrane. Again, this difference could be a result of inherent differences between $A\beta_{42}$ and $A\beta_{40}$. Despite the absence of water leakage, our results still demonstrate considerable structural perturbations induced by $A\beta_{40}$ aggregates, with invaginations that are additive when aggregates form. Thus, it is possible that even larger aggregates, present when $A\beta$ accumulates to higher concentrations, will conduct water and perhaps ions, behavior that has been implicated in neurotoxicity.[51,52]

CONCLUSIONS

We conducted an extensive analysis of $A\beta_{40}$ aggregation in a variety of physiologically relevant model membranes. We found that $A\beta_{40}$ can form aggregates within the membrane and that the interactions between the peptides that lead to the formation of these structures occur exclusively within the N-terminal polar region of the peptide sequence. Secondary structure content in the aggregated species was comparable to that of monomeric $A\beta_{40}$,[10] indicating that more extensive β-strand formation likely only occurs in higher-order membrane-bound aggregates or in aqueous solution. Unlike the $A\beta_{40}$ monomer, aggregated $A\beta_{40}$ did not exit any of the model membranes examined here, in agreement with experimental results that suggest $A\beta$ aggregation within membranes is favored over the monomeric state in solution.[16] We note that, despite the stability within the membrane of the aggregates formed in our simulations, it is possible that aggregated $A\beta$ may leave the membrane over time scales inaccessible to MD simulations. We further find that peptide-induced membrane deformation is strongly dependent upon the lipid content of the model membrane. Whereas the POPC membrane was very susceptible to $A\beta_{40}$-induced defects, lipids that are capable of more extensive interlipid hydrogen bonding (such as POPS and POPE) ameliorated this effect. Further, cholesterol-rich rafts were less susceptible to such deformations as well, in agreement with the results of Qiu et al.[48] The present work provides a greater understanding of the molecular events that lead to the aggregation of $A\beta_{40}$ in physiological membranes, as well as greater detail into the membrane domains that are most susceptible to $A\beta$-induced toxicity.

ASSOCIATED CONTENT

Supporting Information

Thirty figures are provided, showing side-on views of the membrane systems, histograms of relative position data, secondary structure probabilities as a function of $A\beta_{40}$ residue, the complete membrane thickness data sets, and the final configurations of all peptides in these simulations. This material is available free of charge via the Internet at http://pubs.acs.org.

AUTHOR INFORMATION

Corresponding Author

*Phone: (540) 231-5040. Fax: (540) 231-9070. E-mail: jalemkul@vt.edu.

Funding

†This work was supported by the Institute for Critical Technology and Applied Science (ICTAS) at Virginia Tech and in part by NSF grant CNS-0960081 and the HokieSpeed supercomputer at Virginia Tech.

Notes

The authors declare no competing financial interest.

ACKNOWLEDGMENTS

The authors thank the administrators of Advanced Research Computing at Virginia Tech for computing time on the SystemX, Athena, HokieOne, and HokieSpeed supercomputers and XSEDE and the Texas Advanced Computing Center for computing time on the Lonestar, Ranger, and Stampede supercomputers under allocations TG-MCB120137 and TG-MCB120161.

ABBREVIATIONS USED

$A\beta$, amyloid β-peptide; $A\beta_{40}$, 40-residue alloform of $A\beta$; $A\beta_{42}$, 42-residue alloform of $A\beta$; APP, amyloid precursor protein; MD, molecular dynamics; DPPC, dipalmitoylphosphatidylcholine; POPC, palmitoyloleoylphosphatidylcholine; POPS, palmitoyloleoylphosphatidylserine; POPE, palmitoyloleoylphosphatidylethanolamine; PSM, palmitoylsphingomyelin; PME, Particle Mesh Ewald; P-LINCS, Parallel Linear Constraint Solver; COM, center of mass

REFERENCES

(1) Saido, T. C., and Iwata, N. (2006) Metabolism of amyloid β peptide and pathogenesis of Alzheimer's disease: Towards presymptomatic diagnosis, prevention and therapy. *Neurosci. Res. 54*, 235−253.

(2) Hardy, J. A., and Higgins, G. A. (1992) Alzheimer's Disease: The amyloid cascade hypothesis. *Science 256*, 184−185.

(3) Kayed, R., Head, E., Thompson, J. L., McIntire, T. M., Milton, S. C., Cotman, C. W., and Glabe, C. G. (2003) Common structure of soluble amyloid oligomers implies common mechanism of pathogenesis. *Science 300*, 486−489.

(4) Kayed, R., Sokolov, Y., Edmonds, B., McIntire, T. M., Milton, S. C., Hall, J. E., and Glabe, C. G. (2004) Permeabilization of lipid bilayers is a common conformation-dependent activity of soluble amyloid oligomers in protein misfolding diseases. *J. Biol. Chem. 279*, 46363−46366.

(5) Haass, C., and Selkoe, D. J. (2007) Soluble protein oligomers in neurodegeneration: lessons from the Alzheimer's amyloid β-peptide. *Nat. Rev. Mol. Cell Biol. 8*, 101−112.

(6) Thinakaran, G., and Koo, E. H. (2008) Amyloid precursor protein trafficking, processing, and function. *J. Biol. Chem. 283*, 29615−29619.

(7) Hur, J.-Y., Welander, H., Behbahani, H., Aoki, M., Frånberg, J., Winblad, B., Frykman, S., and Tjernberg, L. O. (2010) Active γ-secretase is localized to detergent-resistant membranes in human brain. *FEBS J. 275*, 1174−1187.

(8) Lemkul, J. A., and Bevan, D. R. (2008) A comparative molecular dynamics analysis of the amyloid β-peptide in a lipid bilayer. *Arch. Biochem. Biophys. 470*, 54−63.

(9) Lemkul, J. A., and Bevan, D. R. (2009) Perturbation of membranes by the amyloid β-peptide - a molecular dynamics study. *FEBS J. 276*, 3060−3075.

(10) Lemkul, J. A., and Bevan, D. R. (2011) Lipid composition influences the release of Alzheimer's amyloid β-peptide from membranes. *Protein Sci. 20*, 1530−1545.

(11) Lesné, S., Koh, M. T., Kotilinek, L., Kayed, R., Glabe, C. G., Yang, A., Gallagher, M., and Ashe, K. H. (2006) A specific amyloid-β protein assembly in the brain impairs memory. *Nature 440*, 352−357.

(12) Wasling, P., Daborg, J., Riebe, I., Andersson, M., Portelius, E., Blennow, K., Hanse, E., and Zetterberg, H. (2009) Synaptic Retrogenesis and Amyloid-β in Alzheimer's Disease. *J. Alzheimer's Dis. 16*, 1−14.

(13) Bokvist, M., and Gröbner, G. (2007) Misfolding of amyloidogenic proteins at membrane surfaces: The impact of macromolecular crowding. *J. Am. Chem. Soc. 129*, 14848−14849.
(14) Zhou, H.-X. (2009) Crowding effects of membrane proteins. *J. Phys. Chem. B 113*, 7995−8005.
(15) Bokvist, M., Lindström, F., Watts, A., and Gröbner, G. (2004) Two types of Alzheimer's β-amyloid (1−40) peptide membrane interactions: Aggregation preventing transmembrane anchoring *versus* accelerated surface fibril formation. *J. Mol. Biol. 335*, 1039−1049.
(16) Zhang, Y.-J., Shi, J.-M., Bai, C.-J., Wang, H., Li, H.-Y., Wu, Y., and Ji, S.-R. (2012) Intra-membrane oligomerization and extra-membrane oligomerization of amyloid-β peptide are competing processes as a result of distinct patterns of motif interplay. *J. Biol. Chem. 287*, 748−756.
(17) Chi, E. Y., Ege, C., Winans, A., Majewski, J., Wu, G., Kjaer, K., and Lee, K. Y. C. (2008) Lipid membrane templates the ordering and induces the fibrillogenesis of Alzheimer's disease amyloid-β peptide. *Proteins: Struct. Funct. Bioinform. 72*, 1−24.
(18) Yip, C. M., and McLaurin, J. (2001) Amyloid-β peptide assembly: A critical step in fibrillogenesis and membrane disruption. *Biophys. J. 80*, 1359−1371.
(19) Zhao, L. N., Chiu, S.-W., Benoit, J., Chew, L. Y., and Mu, Y. (2011) Amyloid β peptides aggregation in a mixed membrane bilayer: A molecular dynamics study. *J. Phys. Chem. B 115*, 12247−12256.
(20) Coles, M., Bicknell, W., Watson, A. A., Fairlie, D. P., and Craik, D. J. (1998) Solution structure of amyloid β-peptide(1−40) in a water-micelle environment. Is the membrane-spanning domain where we think it is? *Biochemistry 37*, 11064−11077.
(21) Berger, O., Edholm, O., and Jähnig, F. (1997) Molecular dynamics simulations of a fluid bilayer of dipalmitoylphosphatidylcholine at full hydration, constant pressure, and constant temperature. *Biophys. J. 72*, 2002−2013.
(22) Leekumjorn, S., Wu, Y., Sum, A. K., and Chan, C. (2008) Experimental and computational studies investigating trehalose protection of HepG2 cells from palmitate-induced toxicity. *Biophys. J. 94*, 2869−2883.
(23) Niemelä, P. S., Ollila, S., Hyvönen, M. T., Karttunen, M., and Vattulainen, I. (2007) Assessing the nature of lipid raft membranes. *PLoS Comp. Biol. 3*, e34.
(24) Tieleman, D. P., Forrest, L. R., Sansom, M. S. P., and Berendsen, H. J. C. (1998) Lipid properties and the orientation of aromatic residues in OmpF, influenza M2, and alamethicin systems: Molecular dynamics simulations. *Biochemistry 37*, 17554−17561.
(25) Tieleman, D. P., Sansom, M. S. P., and Berendsen, H. J. C. (1999) Alamethicin helices in a bilayer and in solution: Molecular dynamics simulations. *Biophys. J. 76*, 40−49.
(26) Oostenbrink, C., Villa, A., Mark, A. E., and van Gunsteren, W. F. (2004) A biomolecular force field based on the free enthalpy of hydration and solvation: the GROMOS force-field parameter sets 53A5 and 53A6. *J. Comput. Chem. 25*, 1656−1676.
(27) Kandt, C., Ash, W. L., and Tieleman, D. P. (2007) Setting up and running molecular dynamics simulations of membrane proteins. *Methods 41*, 475−488.
(28) Hess, B., Kutzner, C., van der Spoel, D., and Lindahl, E. (2008) GROMACS 4: Algorithms for highly efficient, load-balanced, and scalable molecular simulation. *J. Chem. Theory Comput. 4*, 435−447.
(29) Berendsen, H. J. C., Postma, J. P. M., van Gunsteren, W. F., and Hermans, J. (1981) Interaction models for water in relation to protein hydration, in *Intermolecular Forces* (Pullman, B., Ed.), p 331, Reidel, Dordrecht.
(30) Berendsen, H. J. C., Postma, J. P. M., van Gunsteren, W. F., DiNola, A., and Haak, J. R. (1984) Molecular dynamics with coupling to an external bath. *J. Chem. Phys. 81*, 3684−3690.
(31) Hoover, W. G. (1985) Canonical dynamics: Equilibrium phase-space distributions. *Phys. Rev. A: At., Mol., Opt. Phys. 31*, 1695−1697.
(32) Nosé, S. (1984) A unified formulation of the constant temperature molecular dynamics methods. *J. Chem. Phys. 81*, 511−519.
(33) Nosé, S., and Klein, M. L. (1983) Constant pressure molecular dynamics for molecular systems. *Mol. Phys. 50*, 1055−1076.
(34) Parrinello, M., and Rahman, A. (1981) Polymorphic transitions in single crystals: A new molecular dynamics method. *J. Appl. Phys. 52*, 7182−7190.
(35) Hess, B. (2008) P-LINCS: A parallel linear constraint solver for molecular simulation. *J. Chem. Theory Comput. 4*, 116−122.
(36) Darden, T., York, D., and Pedersen, L. (1993) Particle mesh Ewald: an N·log(N) method for Ewald sums in large systems. *J. Chem. Phys. 98*, 10089−10092.
(37) Essmann, U., Perera, L., Berkowitz, M. L., Darden, T., Lee, H., and Pedersen, L. G. (1995) A smooth particle mesh Ewald method. *J. Chem. Phys. 103*, 8577−8593.
(38) Allen, W. J., Lemkul, J. A., and Bevan, D. R. (2009) GridMAT-MD: A grid-based membrane analysis tool for use with molecular dynamics. *J. Comput. Chem. 30*, 1952−1958.
(39) Kabsch, W., and Sander, C. (1983) Dictionary of protein secondary structure: Pattern recognition of hydrogen-bonded and geometrical features. *Biopolymers 22*, 2577−2637.
(40) Best, R. B., Buchete, N.-V., and Hummer, G. (2008) Are current molecular dynamics force fields too helical? *Biophys. J. 95*, L07−L09.
(41) Matthes, D., and de Groot, B. L. (2009) Secondary structure propensities in peptide folding simulations: A systematic comparison of molecular mechanics interaction schemes. *Biophys. J. 97*, 599−608.
(42) Olubiyi, O. O., and Strodel, B. (2012) Structures of the amyloid β-peptides Aβ_{1-40} and Aβ_{1-42} as influenced by pH and a D-peptide. *J. Phys. Chem. B 116*, 3280−3291.
(43) Crescenzi, O., Tomaselli, S., Guerrini, R., Salvadori, S., D'Ursi, A. M., Temussi, P. A., and Picone, D. (2002) Solution structure of the Alzheimer amyloid β-peptide (1−42) in an apolar microenvironment. *Eur. Biophys. J. 269*, 5642−5648.
(44) Sticht, H., Bayer, P., Willbold, D., Dames, S., Hilbich, C., Beyreuther, K., Frank, R. W., and Rösch, P. (1995) Structure of amyloid A4-(1−40)-peptide of Alzheimer's disease. *Eur. Biophys. J. 233*, 293−298.
(45) Xu, Y., Shen, J., Luo, X., Zhu, W., Chen, K., Ma, J., and Jiang, H. (2005) Conformational transition of amyloid β-peptide. *Proc. Natl. Acad. Sci. U.S.A. 102*, 5403−5407.
(46) Best, R. B., and Hummer, G. (2009) Optimized molecular dynamics force fields applied to the helix-coil transition of polypeptides. *J. Phys. Chem. B 113*, 9004−9015.
(47) Roychaudhuri, R., Yang, M., Hoshi, M. M., and Teplow, D. B. (2009) Amyloid β-protein assembly and Alzheimer Disease. *J. Biol. Chem. 284*, 4749−4753.
(48) Qiu, L., Buie, C., Reay, A., Vaughn, M. W., and Cheng, K. H. (2011) Molecular dynamics simulations reveal the protective role of cholesterol in β-amyloid protein-induced membrane disruptions in neuronal membrane mimics. *J. Phys. Chem. B 115*, 9795−9812.
(49) Verdier, Y., Zarándi, M., and Penke, B. (2004) Amyloid β-peptide interactions with neuronal and glial cell plasma membrane: Binding sites and implications for Alzheimer's Disease. *J. Pept. Sci. 10*, 229−248.
(50) Poojari, C., Kukol, A., and Strodel, B. (2013) How the amyloid-β peptide and membranes affect each other: An extensive simulation study. *Biochim. Biophys. Acta, Biomembr. 1828*, 327−339.
(51) Arispe, N., Rojas, E., and Pollard, H. B. (1993) Alzheimer disease amyloid β forms calcium channels in bilayer membranes: Blockade by tromethamine and aluminum. *Proc. Natl. Acad. Sci. U.S.A. 90*, 567−571.
(52) Capone, R., Quiroz, F. G., Prangkio, P., Saluja, I., Sauer, A. M., Bautista, M. R., Turner, R. S., Yang, J., and Mayer, M. (2009) Amyloid-β-Induced ion flux in artificial lipid bilayers and neuronal cells: Resolving a controversy. *Neurotox. Res. 16*, 1−13.